Analysis of the Movement of *Chlamydomonas* Flagella: The Function of the Radial-spoke System Is Revealed by Comparison of Wild-type and Mutant Flagella

C. J. BROKAW, D. J. L. LUCK, and B. HUANG
Division of Biology, California Institute of Technology, Pasadena, California 91125, and The Rockefeller University, New York 10021

ABSTRACT The mutation *uni*-1 gives rise to uniflagellate *Chlamydomonas* cells which rotate around a fixed point in the microscope field, so that the flagellar bending pattern can be photographed easily. This has allowed us to make a detailed analysis of the wild-type flagellar bending pattern and the bending patterns of flagella on several mutant strains. Cells containing *uni*-1, and recombinants of *uni*-1 with the suppressor mutations, sup_{pf}-1 and sup_{pf}-3, show the typical asymmetric bending pattern associated with forward swimming in *Chlamydomonas*, although sup_{pf}-1 flagella have about one-half the normal beat frequency, apparently as the result of defective function of the outer dynein arms. The *pf*-17 mutation has been shown to produce nonmotile flagella in which radial spoke heads and five characteristic axonemal polypeptides are missing. Recombinants containing *pf*-17 and either sup_{pf}-1 or sup_{pf}-3 have motile flagella, but still lack radial-spoke heads and the associated polypeptides. The flagellar bending pattern of these recombinants lacking radial-spoke heads is a nearly symmetric, large amplitude pattern which is quite unlike the wild-type pattern. However, the presence of an intact radial-spoke system is not required to convert active sliding into bending and is not required for bend initiation and bend propagation, since all of these processes are active in the sup_{pf} *pf*-17 recombinants. The function of the radial-spoke system appears to be to convert the symmetric bending pattern displayed by these recombinants into the asymmetric bending pattern required for efficient swimming, by inhibiting the development of reverse bends during the recovery phase of the bending cycle.

Chlamydomonas has proven to be a valuable organism for genetic and biochemical investigations of flagellar structure. Flagellar function in *Chlamydomonas* has received more limited attention, in part because of the difficulty of observing or photographically recording the activity of flagella on swimming cells. We describe here an analysis of the movement of *Chlamydomonas* flagella, which has been facilitated by making use of a mutant *uni*-1 (B. Huang, Z. Ramanis, S. Dutcher, and D. J. L. Luck, manuscript in preparation). In *uni*-1 a high proportion of cells are uniflagellate. When flagella beat in the asymmetric or "breast-stroke" mode which propels biflagellate cells forward, *uni*-1 cells rotate, and in most cases the cells show little precession. The flagellar beat is executed in a plane perpendicular to the axis of rotation, and the bending cycle of cells in which the bending plane is stabilized by proximity to the surface of a microscope slide can be recorded easily by stroboscopic dark-field microscopy. We have used this method to analyze the normal, wild-type, "breast-stroke" mode of flagellar beating, and one type of variant beating pattern associated with a flagellar motility mutation.

Among the "paralyzed" flagellar mutants isolated from *Chlamydomonas reinhardtii*, which show little or no flagellar motility, are several mutants in which morphological and/or molecular defects in the radial-spoke or central-pair microtubule structures of the axoneme have been observed (1, 14, 19, 28, 29). The force generating components of the axoneme, the inner and outer dynein arms, appear to be intact in these mutants, and in some cases ATP-driven sliding disintegration of trypsin-digested mutant axonemes has been demonstrated (30). An apparently similar axonemal state in which flagellar bending is inhibited while the active sliding mechanism appears to be intact can also be obtained in flagella inhibited by CO_2

THE JOURNAL OF CELL BIOLOGY · VOLUME 92 MARCH 1982 722-732

(8), anti-tubulin antibodies (2), or Ni^{2+} ions (17). In the case of Ni^{2+} ion inhibition, and also in the case of flagella exposed to very low $MgATP^{2-}$ concentrations (24), it has been shown that bend propagation can occur under conditions where bend initiation is suppressed. This axonemal state is interesting because it may indicate the malfunctioning of still unknown mechanisms that may be required to inhibit selectively the active sliding process in particular regions of the axoneme to obtain the non-uniform active sliding required for flagellar bending. The occurrence of this state in association with morphological defects in the radial-spoke or central-pair microtubule structures provided a strong suggestion that radial spoke–central pair interactions might be important in modulating the activity of the dynein arm active sliding mechanism, which was also suggested by ultrastructural evidence for cyclic changes in these interactions during the ciliary bending cycle (27).

A reevaluation of this suggestion is now required by the discovery of suppressor mutations (sup_{pf}) which restore motility to radial-spoke and/or central-pair defective paralyzed mutants without altering their molecular or morphological defects (15). Four sup_{pf} mutants, representing different chromosomal loci, have been characterized. sup_{pf}-1 and sup_{pf}-2 restore flagellar activity to both central-pair and radial-spoke defective mutants, while sup_{pf}-3 and sup_{pf}-4 restore activity only to radial-spoke defective mutants. The data here constitute an analysis of flagellar bending cycles in the forward mode, in wild type, in strains carrying the sup_{pf}-1 and sup_{pf}-3 mutations alone, and in recombinants of these two suppressors with the mutant *pf*-17. Each observation has been made in the background of the *uni*-1 mutation. The paralyzed mutant *pf*-17 shows no flagellar activity, except for an occasional twitch.

MATERIALS AND METHODS

Cells of *Chlamydomonas reinhardtii* were scraped from culture plates and suspended in nitrogen-free medium (18) to induce formation of flagellated gametic cells. After 1–3 h, these cells were collected by gentle centrifugation and resuspended in a solution containing 1 mM KCl, 2 mM EGTA, 1.7 mM $CaCl_2$, 0.1 mM $MgCl_2$, and 5 mM HEPES buffer, at pH 7.1. This solution has a relatively low Ca^{2+} ion concentration ($\sim 10^{-6}$ M), but the exact value will vary depending on the amount of culture solution transferred with the cells. It was used to suppress the flagellar reversal reaction which depends on the presence of Ca^{2+} in the medium (3, 23).

A 25-μl portion of this cell suspension was placed on a clean microscope slide and a cover glass was added. Slides and cover glasses were routinely rinsed with ethanol and dried with a pad of Kimwipes. Flagellar movement was observed and photographed using a × 40 oil immersion objective and a dark-field condenser, with a magnification on 35mm Tri-X film of × 160. Illumination was provided by a Varian VIX-150F xenon arc lamp (Eimac Division, Varian Associates, San Carlos, CA) powered in a pulsed mode with a Chadwick Helmuth model 136 power supply (Chadwick Helmuth Corp., El Monte, CA). Moving film photography with a modified Robot camera (5) was used to separate images on film so that multiple images of the cell body did not obscure the basal portion of the flagellum. Flash frequencies were measured by a General Radio model 1192B frequency counter (GenRad Inc., Concord, MA), which measured the period between flash trigger pulses to 0.1 ms, and were recorded manually. All data was recorded using a microscope stage maintained at 25°C by circulating water from a thermostated bath.

Cells were selected for photography that were rotating consistently, with the flagellum beating in a plane parallel to the microscope-slide surface. In most cases, the flash frequency was adjusted to a value somewhat below the flagellar beat frequency, so that a circular pattern of flagellar images that appeared to contain two to three complete beat cycles was seen as the cell rotated. This gave photographs that appeared to contain five to 10 images per beat cycle; actually, because of the "stroboscopic" effect, a sequence of images that appeared to repeat every n^{th} image corresponded to n+1 beat cycles, with images occurring at times separated by 1+1/n beat cycles. The beat frequency is then equal to 1+1/n times the flash frequency. sup_{pf}-1*pf*-17 recombinants had beat frequencies sufficiently low for photography at flash rates much higher than the beat frequency. Flash rates of 50, 60, or 70 Hz were used for these, and the photographs contained multiple images within individual flagellar beat cycles.

Image analysis was performed by projecting the negatives onto the screen of a microfilm reader at a final magnification of × 3,650. x and y coordinates of points on the center line of a flagellar image were obtained using a Numonics model 1220 digitizer (Numonics Corp., Lansdale, PA) in point-to-point mode and transmitted to a HP85 microcomputer (Hewlett-Packard Co., Corvallis, Oregon). The computer determined the angle and distance between each pair of points entered, and then converted this information to give the angular orientation of the flagellum as a function of flagellar length at uniform intervals (corresponding to 0.4 μm) along the length. Repeated tracings (two to six) of each image were averaged to minimize the effects of measurement errors and produce smoother curves. The inherent resolution of the digitizer is 0.25 mm, but repeated measurements of a fixed distance typically had standard deviations (SD) of ~0.1 mm. Since the projected image of the flagellum was typically ~1.5 mm wide, the accuracy of the data was largely limited by image quality and determination of the midline of the flagellar image, rather than by the precision of the digitizer.

One type of error is not reduced by averaging repeated tracings. These are cumulative errors in the measurement of length along the flagellum. In a curved region of the flagellum, the arc length is approximated by a chord between two x,y points. The maximum curvatures encountered with the *Chlamydomonas* flagellar images were ~1 radian/μm, for short regions near the base of the flagellum. If the x,y points are measured at intervals corresponding to 0.5 μm, the length will be underestimated by 1% when the curvature is this large. On the other hand, an overestimation of length will result from the summation of the length of straight segments between points that do not lie exactly on the center line of the flagellum. If the error is on the order of the inherent resolution of the digitizer, e.g., 0.25 mm or 0.07 μm, and x,y points are measured at intervals corresponding to 0.5 μm, the error will be on the order of +1%. This error will be greater if shorter segment lengths are used between x,y points. To minimize it, the microcomputer was instructed to reject points that corresponded to a distance of <0.3 μm from the previously entered point and to request the operator to reenter that point. This limitation also limited fluctuations in the angles of the line segments connecting successive points. These two cumulative errors tend to neutralize each other in curved regions measured with relatively short steps; in straighter regions the distance between measured points was usually increased to reduce the overestimation of length. We are therefore satisfied that this type of error can be neglected in our analysis.

The data on angle as a function of length along the flagellum was stored on magnetic tape, and used later to generate composite plots for multiple images of a flagellum, as in Fig. 2*A*. Integration of the angle vs. length data was used to regenerate and plot multiple x,y images of the flagellar bending pattern, as in Fig. 2*B*.

At the start of analysis of images for a particular cell, the film was rotated so that the long axis of a cell body image was aligned with the *x*-coordinate axis of the digitizer. A water-color pen was used to trace the outline of the cell body and any obvious features of the cell morphology on the projection screen. A point corresponding to the approximate position of the basal end of the flagellum was also marked on the projection screen, and used as the origin for x,y coordinate measurements. For analysis of subsequent images of the same cell, the film was repositioned so that the image of the cell body was aligned with the tracing on the screen. This procedure established the coordinates used for the results shown in Figs. 2–5. The absolute origins of these coordinate axes are only rough estimates of the position and orientation of the basal end of the flagellum. The relative positions of the curves, although dependent on the accuracy of positioning each image, should be significant.

RESULTS

Photographic Data

Fig. 1 illustrates the type of photograph obtained for each cell type analyzed in this paper. Fig. 1*A* illustrates the normal wild-type flagellar behavior shown by flagella on cells containing only the mutation *uni*-1 in an otherwise wild-type background. All other data in this paper are also from cells containing *uni*-1, even when this is not explicitly mentioned. Fig. 1*B* and *C* illustrate the behavior of flagella on cells containing a suppressor mutation, sup_{pf}-3 or sup_{pf}-1. In both cases, the flagellar behavior appears similar to the normal beat cycle, although the beat frequency is consistently lower in the case of sup_{pf}-1. Fig. 1*D* and *E* illustrate the behavior of flagella on cells containing one of these suppressors and the paralyzed flagellar mutation *pf*-17. In these cases, the flagellar behavior is clearly different from the normal beat cycle, but the patterns obtained with the two different suppressors appear to be simi-

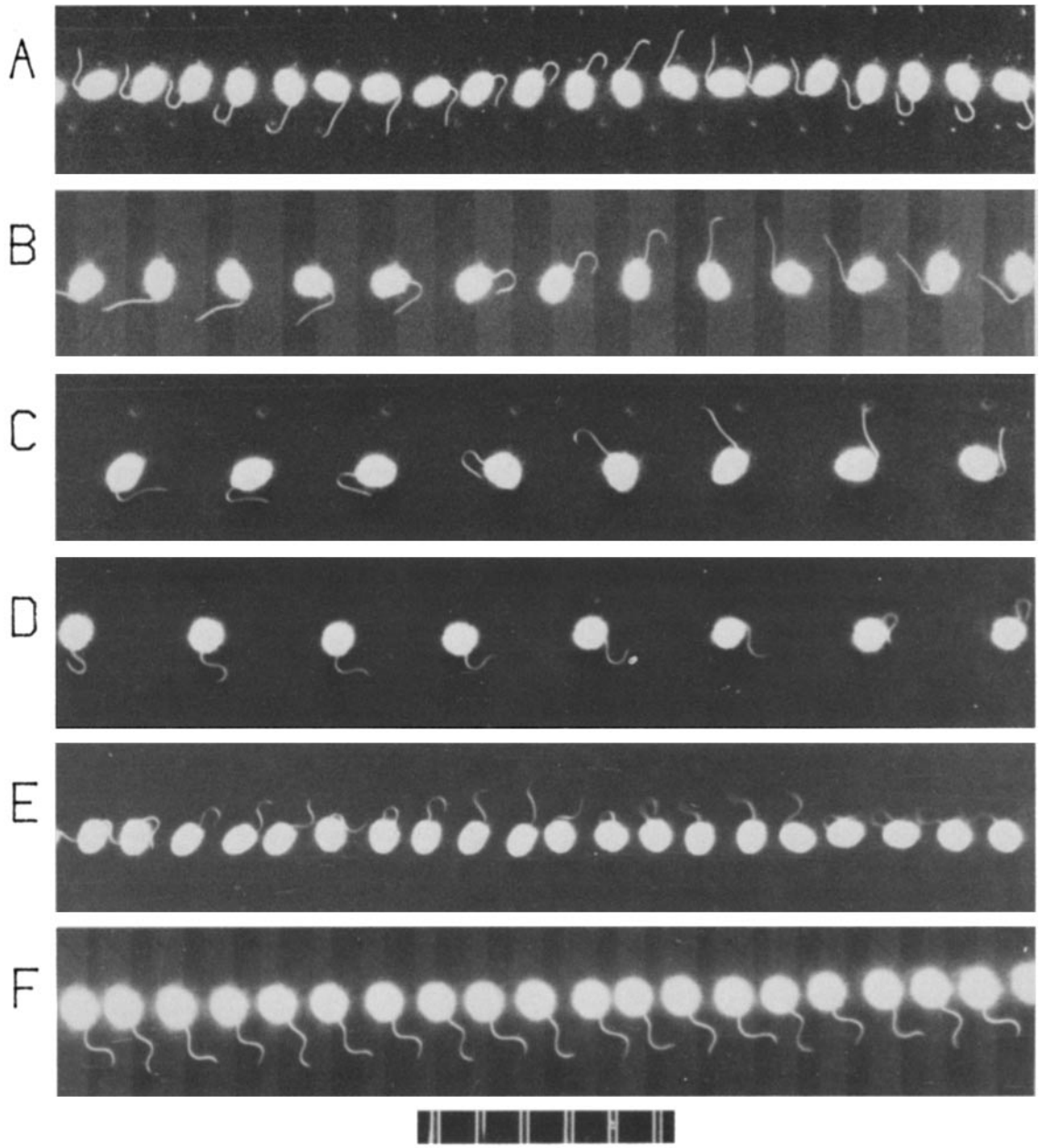

FIGURE 1 Examples of the photographs used for analysis of the movement of *Chlamydomonas* flagella. All prints show time sequences from left to right; the scale divisions are 10 μm. (*A*) Wild-type bending pattern; flash rate 69.0 Hz. (*B*) A cell containing the suppressor mutation sup_{pf}-3; flash rate 49.3 Hz. (*C*) A cell containing the suppressor mutation sup_{pf}-1; flash rate 26.7 Hz. (*D*) A cell containing the paralyzed flagellar mutation *pf*-17 and sup_{pf}-3; flash rate 23.9 Hz. (*E*) A cell containing the paralyzed flagellar mutation *pf*-17 and sup_{pf}-1; flash rate 70 Hz. (*F*) Bending pattern during the flagellar reversal reaction; wild-type cell; flash rate 56.2 Hz.

lar. Fig. 1*f* illustrates the "reversal" behavior of a flagellum on a cell which is wild-type except for the uniflagellar mutation *uni*-1. The low-calcium medium used for these experiments was used to discourage the calcium-dependent (3, 23) reversal responses and no detailed analysis of this bending pattern has yet been made. However, the photograph is included here to demonstrate that this symmetrical bending pattern is clearly distinct from the bending patterns of the suppressed *pf*-17 flagella illustrated in Fig. 1 *D* and *E*.

Analysis of the Normal Beat Cycle

Plots of angle vs. length along the flagellum for a flagellum executing a wild-type (*wt*) beat cycle are shown in Fig. 2*A*. If the base of the flagellum is assumed to be rigidly anchored in the cell body, if it is assumed that no sliding between flagellar tubules can occur at the basal end of the flagellum, and if there is no significant twisting of the axoneme, curves such as those in Fig. 2*A* can be interpreted as "shear curves" (5) that provide an angular measure of the amount of shear displacement between flagellar tubules as a function of length along the flagellum. The vertical distance between successive shear curves then gives an estimate of the shear rate, or sliding velocity, between tubules, averaged over the time interval between images. However, this estimate is highly sensitive to errors in determining the orientation of the cell body when tracing images of the flagellum. In addition, because of the

stroboscopic method used to obtain these flagellar images, any irregularities in beat frequency will also influence the estimates of shear rates between successive shear curves.

The data in the shear curves (Fig. 2*A*) can be integrated to reconstruct the image of the flagellum in an x,y coordinate plane and illustrate the bending pattern with the cell body rotation factored out. The result of this process is shown in Fig. 2*b*. (This bending pattern is unlikely to be identical to the bending pattern generated by a flagellum on a stationary cell, as the hydrodynamic loading is different for rotating and stationary cells.) Since the shear curves contain data averaged from several independent tracings of the flagellar images, the reconstructed x,y curves also represent data averaged from several tracings, and may therefore be better representations of the flagellar configurations than can be obtained from simple tracings of the images. A similar reconstruction process was used by Hiramoto and Baba (12) in their study of the waveforms of echinoderm sperm flagella, although their averaging process operated on curvatures rather than angles.

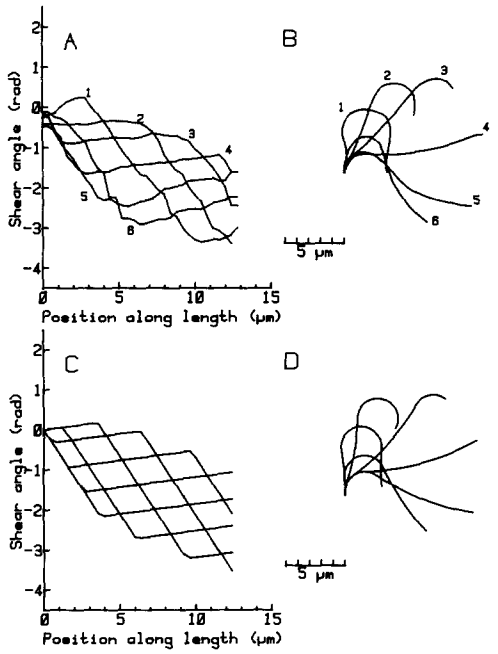

FIGURE 2 Analysis of a wild-type bending pattern. (*A*) Shear curves generated by repeated tracings of six consecutive images of this flagellum. (*B*) Bending pattern reconstructed by integration of the shear curves in *A*. (*C*) Artificial shear curves constructed according to a "constant curvature" model for the bending pattern, using data obtained from shear curves in *A*. (*D*) Artificial bending pattern constructed by integration of the shear curves in *C*. Data for this flagellum are given in column 1 of Table I.

Inspection of shear curves such as Fig. 2*A* suggests that the waveform is constructed of relatively distinct bent regions, corresponding to regions of constant slope in the shear curves, in which curvature and sliding velocity are relatively uniform. These bent regions are separated by relatively short transition regions, in which the curvature passes through 0, but does not remain equal to 0 to produce "straight regions" between bends. This inspection suggests that it may be possible to characterize the major features of a bending pattern by specifying the curvature and sliding velocity in each bend. In doing this, it is convenient to use the terminology introduced for describing asymmetrical bending patterns of sea urchin sperm flagella (9). The bend of larger curvature which is formed at the base of the flagellum during the "effective stroke" is referred to as the principal bend. The principal bends are the regions of large, negative slope in the shear curves. The bends in the opposite direction are termed reverse bends; they correspond to the regions of small, positive slope in the shear curves.

The average curvature in the principal and reverse bends, denoted by κ_P and κ_R respectively, can be estimated from the shear curves, as well as the average shear rates in the principal and reverse bends, denoted by V_P and V_R, respectively, when measured in radians per beat cycle. In addition to these four parameters, it is necessary to specify a fifth parameter, τ, which is the fraction of the beat period between the initiation of sliding in the reverse bend and the initiation of sliding in the principal bend. For example, in the flagellum shown in Fig. 2, there are six images per beat cycle. In images 3, 4, and 5, there is a principal bend at the base of the flagellum, which increases in length while its curvature remains approximately constant. No sliding occurs in this bend between images 3 and 4 or between images 4 and 5, so it remains at the base of the flagellum without propagating. In image 6, this principal bend has begun to propagate along the flagellum as a result of sliding which begins in the principal bend some time between images 5 and 6. This sliding also causes the appearance of a new

TABLE I
Data for Individual Flagella

Type		wt	wt	wt	sup_{pf}−3	sup_{pf}−1	sup_{pf}−3 *pf*−17	sup_{pf}−3 *pf*−17	sup_{pf}−1 *pf*−17
Shown in Figure:		2	3 *a* and *b*	3 *c* and *d*	4 *a*	4 *b*	5 *a*	5 *b*	5 *c*
Flagellar length (*μm*)		12.4	12.4	12.4	12.8	10.4	12	13.2	11.4
Beat frequency (*Hz*)	f:	67	54	77	53	33	36	42	11.5
Time interval*	τ:	0.66	0.6	0.5	0.5	0.45	0.5	0.5	0.56
Curvature in principal bends, *Radians/μm*	κ_P:	0.58	0.57	0.58	0.55	0.66	0.55	0.51	0.56
Curvature in reverse bends, *Radians/μm*	κ_R:	0.05	0.10	0.04	0.06	0.12	0.27	0.16	0.49
Rate of sliding in principal bends									
Radians/cycle	V_P:	8.6	9.0	4.8	7.0	6	9.0	7.25	12.0
Radians/s	$\dot{\sigma}_P$:	576	486	370	371	198	324	305	138
Rate of sliding in reverse bends									
Radians/cycle	V_R:	4.0	5.7	3.8	4.7	5.4	7.9	6.4	12
Radians/s	$\dot{\sigma}_R$:	268	308	293	249	178	284	267	138

* The interval between initiation of sliding in reverse bend and initiation of sliding in principal bend (fraction of beat period).

reverse bend at the base of the flagellum, although it is not really apparent until image 1. In image 2, sliding within the new reverse bend has begun. The amounts of sliding between images 1 and 2, and between images 5 and 6, appear to be approximately equal fractions of the average amount of sliding between images, suggesting that the starting points are similarly spaced following images 1 and 5. Therefore, since the interval between images 1 and 5 represents ⅔ of the beat cycle, in this case the estimated value of τ is 0.66. Data obtained from the shear curves in Fig. 2 are summarized in column 1 of Table I. In addition to the five parameters that describe the form of the bending pattern, the flagellar length and the beat frequency, f, are also required to completely characterize this flagellum. It is also useful to express the sliding velocity in absolute terms, radians per second, by multiplying the sliding velocity in radians per cycle by the beat frequency.

As a test of the adequacy of this characterization of the beat pattern, the HP85 microcomputer was programmed to draw shear curves and x,y images for a model flagellum, using as input only the flagellar length and the five bending pattern parameters, κ_P, κ_R, V_P, V_R, and τ. This procedure assumes a "constant curvature" model of flagellar waveforms used in an earlier analysis of asymmetric waveforms of sea urchin sperm flagella (5). An example of the results obtained from this procedure, using data for the flagellum in Fig. 2 *A* and *B*, is shown in Fig. 2 *C* and *D*. Although there is certainly fine detail in the real shear curves, especially in the transitions between bends, that is not reproduced in the model calculations, this procedure generates bending patterns that appear to contain the major features of the *Chlamydomonas* flagellar beat cycle. Since the model shear curves are generated on a relatively transparent paper, it is possible to make a direct comparison of the model shear curves with the shear curves obtained from the data, when the two sets of curves are superimposed. We found that to obtain model shear curve patterns that closely matched the shear curves obtained from the data, it was usually necessary to adjust the values of V_R, V_P, and τ that had been initially estimated from inspection of the shear curves. This procedure was therefore used routinely to obtain a more accurate estimate of parameters for each flagellum that was analyzed.

This analysis was carried out for a sample of 11 flagella on wild-type cells, and the combined data are given in Table II. In forming this sample, photographs of cells having relatively elongated cell bodies were selected, to make orientation of the images more accurate. The relatively small SD for the two values of curvature, κ_P and κ_R, are noteworthy. In contrast, there are relatively large variations in the values of shear rate,

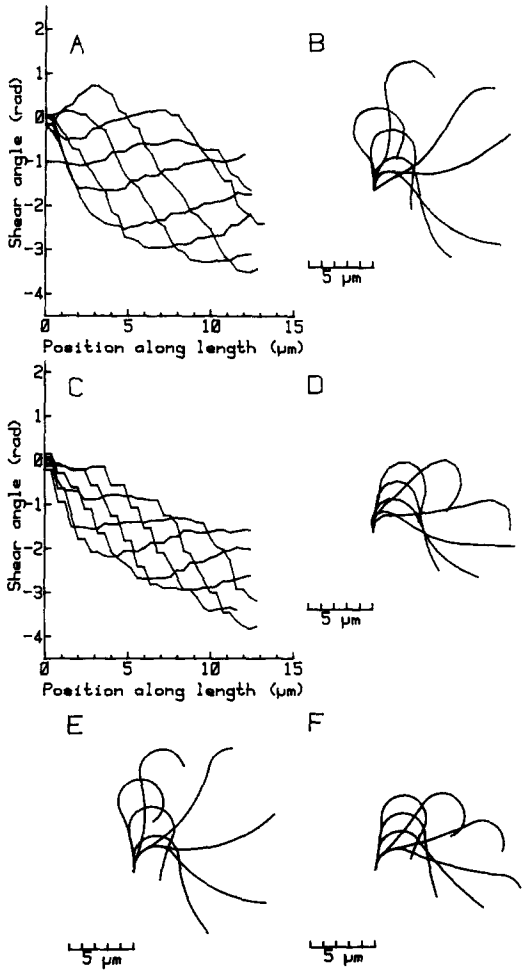

FIGURE 3 Analysis of two wild-type bending patterns showing extreme variations in bend angle. The shear curves for these two flagella are shown in *A* and *C*. *B* is a bending pattern reconstructed from the shear curves in *A*, and *E* is an artifical bending pattern constructed from data extracted from the shear curves in *A*. *D* is a bending pattern reconstructed from the shear curves in *C*, and *F* is an artifical bending pattern constructed from data extracted from the shear curves in *C*.

TABLE II

Data for Flagellar Samples: Means and SD

Type		wt	sup_{pf}−3	sup_{pf}−1	sup_{pf}−3 *pf*−17	sup_{pf}−1 *pf*−17
Shown in Fig. 6		*a*	*b*	*c*	*d*	*e*
Number of flagella measured		11	9	11	15	14
Flagellar length (μm)		12.8 (1.0)	11.8 (1.1)	10.8 (1.9)	11.6 (1.3)	10.4 (1.3)
Beat frequency (*Hz*)	f:	65 (10)	56.4 (4.2)	32.7 (1.8)	35.0 (4.1)	12.1 (2.6)
Time interval*	τ:	0.56 (0.06)	0.56 (0.06)	0.55 (0.11)	0.53 (0.07)	0.52 (0.07)
Curvature in principal bends, *Radians/μm*	κ_P:	0.58 (0.03)	0.60 (0.06)	0.65 (0.07)	0.54 (0.07)	0.55 (0.06)
Curvature in reverse bends, *Radians/μm*	κ_R:	0.06 (0.02)	0.05 (0.02)	0.09 (0.03)	0.26 (0.09)	0.40 (0.10)
Rate of sliding in principal bends						
Radians/cycle	V_P:	7.3 (1.4)	7.0 (0.8)	7.5 (1.1)	9.1 (1.8)	12.8 (3.0)
Radians/s	$\dot{\sigma}_P$:	464 (80)	394 (49)	246 (33)	314 (51)	148 (16)
Rate of sliding in reverse bends						
Radians/cycle	V_R:	4.2 (0.7)	4.4 (0.4)	4.8 (1.1)	7.4 (1.4)	13.0 (3.5)
Radians/s	$\dot{\sigma}_R$:	272 (44)	247 (29)	157 (33)	256 (48)	151 (26)

* The interval between initiation of sliding in reverse bend and initiation of sliding in principal bend (fraction of beat period).

which correspond to variations in the amplitude of the bending patterns of individual flagella. Shear curves and bending patterns for two flagella representing relatively extreme variations in amplitude within this sample are shown in Fig. 3, and the data for these two flagella are given in the second and third data columns in Table I. In addition, Fig. 3 *E* and *F* show the bending patterns reconstructed from the data using the constant curvature model for these two flagella, to show that this modeling procedure adequately characterizes the difference between these two bending patterns. There is also considerable variation in beat frequency. For the two extreme cases shown in Fig. 3, the data (Table I) show an inverse correlation between beat frequency and shear rate per beat cycle, which reduces the variation in absolute shear rate, $\dot{\sigma}$. However, for the sample as a whole (Table II) this correlation was weak, and the relative standard deviations for absolute shear rates were similar to those for shear rates per beat cycle.

Analysis of the Beat Cycles of Flagella on Cells Containing Suppressor Mutations

Similar procedures were used to analyze photographs of flagella on cells containing the suppressor mutations sup_{pf}-3 or sup_{pf}-1. Examples of tracings of individual cells are shown in Fig. 4. Averaged data for the samples of each suppressor are given in Table II. The only difference between the movement of flagella on cells containing a suppressor mutation and flagella on wild-type cells that we consider significant is the reduced beat frequency of flagella on cells containing sup_{pf}-1, which is ~½ the wild-type frequency.

The beat frequencies for cells containing sup_{pf}-3 are slightly lower than the wild-type value. The frequencies obtained with this suppressor fall in the lower range of the values measured in the wild-type sample, which contained cells with flagellar beat frequencies ranging from 50 to 80 Hz. Because of this large range, a more thorough study would be required to determine if there is any difference in beat frequency caused by the presence of this suppressor mutation.

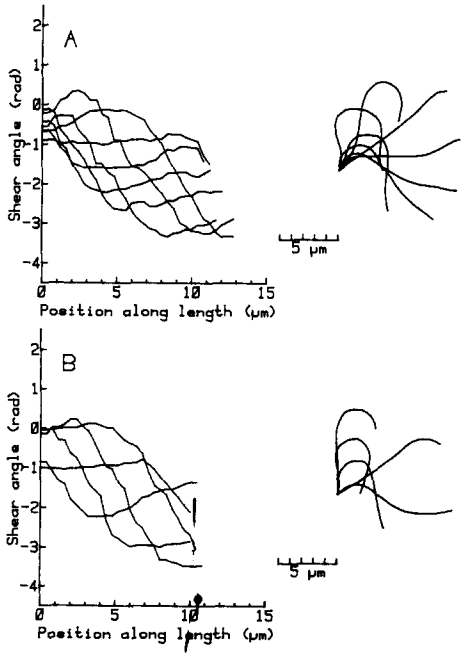

FIGURE 4 Shear curves and reconstructed bending patterns for examples of the suppressor mutations. *A* is from a cell containing sup_{pf}-3. *B* is from a cell containing sup_{pf}-1.

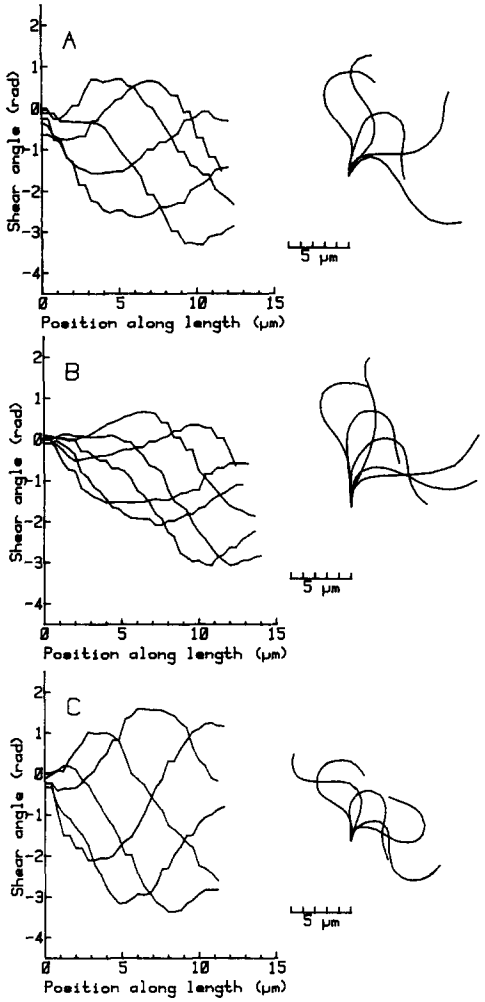

FIGURE 5 Shear curves and reconstructed bending patterns for examples of cells containing the paralyzed flagella mutation, *pf*-17, and a suppressor mutation. *A* and *B* are from cells containing sup_{pf}-3. *C* is from a cell containing sup_{pf}-1.

The curvature in the principal bends (κ_P) of flagella on cells containing sup_{pf}-1 is slightly higher than the wild-type value. If this difference is significant, it may be associated with the slightly shorter lengths measured for the sample of cells containing this suppressor, since the highest values of κ_P were found on cells with flagella shorter than 10 μm, none of which were found in the wild-type sample.

Analysis of the Beat Cycles of Flagella on Cells Containing pf-17 and a Suppressor

Similar procedures were used to analyze photographs of flagella on cells containing the paralyzed flagella mutation, *pf*-17, and one of the two suppressor mutations. Examples of shear curves and bending patterns for individual flagella are shown in Fig. 5. The example shown in Fig. 5 *B* was selected to show one of the mutant bending patterns that most closely resembled the wild-type bending pattern. Averaged data for samples of these sup_{pf} *pf*-17 recombinants are given in the last two columns of Table II.

The obvious difference between the data obtained for cells containing the mutation *pf*-17 and for the other cells is the larger values for curvature in the reverse bends. In the case of cells containing sup_{pf}-3, the presence of the *pf*-17 mutation

increases κ_R, but causes no significant change in κ_P. In the case of cells containing sup_{pf}-1, the presence of the *pf*-17 mutation causes a larger increase in κ_R, and may also cause a small decrease in κ_P. The probability that this difference in κ_P is significant, using a standard Student's *t* test, is only 0.85; however, in this case the average flagellar lengths are similar.

The increased values of κ_R found in the presence of *pf*-17 are associated with reduced beat frequencies and with increased values for the rates of sliding, when expressed in terms of radians per beat cycle. However, it is noteworthy that the presence of the *pf*-17 mutation causes no change in the absolute rate of sliding in the reverse bends, as shown by the bottom line of Table II.

Fig. 6 summarizes the data in Table II in the form of reconstructed bending patterns using the constant curvature model and the averaged data for each of the 5 samples we analyzed. These diagrams, and the data in Table II, reveal a major alteration in the bending pattern associated with the suppressed *pf*-17 mutation, compared with wild-type or the suppressors alone.

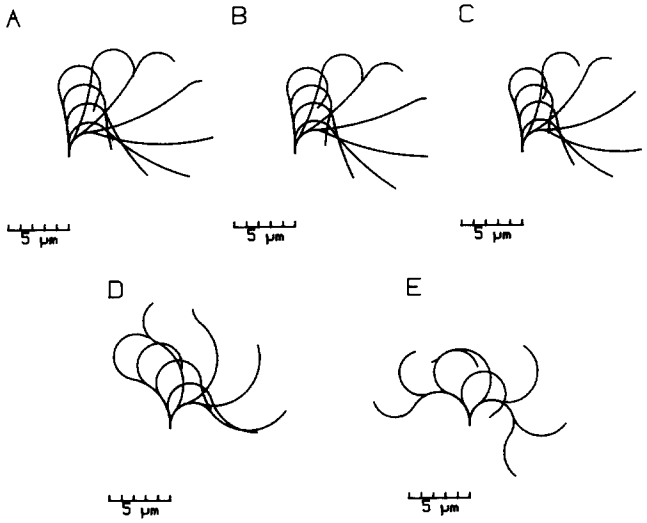

FIGURE 6 Artificial bending patterns constructed from the averaged data in Table II, obtained from the shear curves of flagella in each sample. (*A*) Wild-type cells. (*B*) Cells containing sup_{pf}-3. (*C*) Cells containing sup_{pf}-1. (*D*) Cells containing sup_{pf}-3 *pf*-17. (*E*) Cells containing sup_{pf}-1 *pf*-17.

Molecular Analysis of Flagella on Cells Containing pf-17 and a Suppressor

To establish that the sup_{pf} *pf*-17 *uni*-1 recombinants were lacking radial-spokeheads, we studied the same recombinant

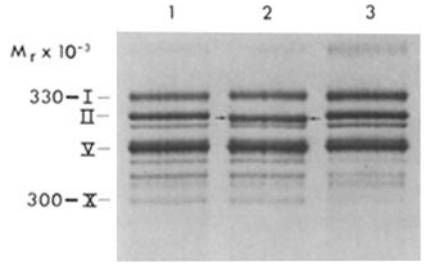

FIGURE 8 Autoradiogram of the polyacrylamide gel slab used for one-dimensional electrophoretic separation of axonemal polypeptides of 300,000 to 400,000 mol wt (methods are given in reference 20). Only the relevant portion of the original gel is shown. Polypeptides, I, II, V, and X are known to be deficient in mutants lacking outer dynein arms (13). (Lane *1*) *uni*-1 axonemes; (Lane *2*) sup_{pf}-1 *pf*-17 *uni*-1·7B axonemes; (Lane *3*) sup_{pf}-3 *pf*-17 *uni*-1·1B axonemes. Additional description is given in the text.

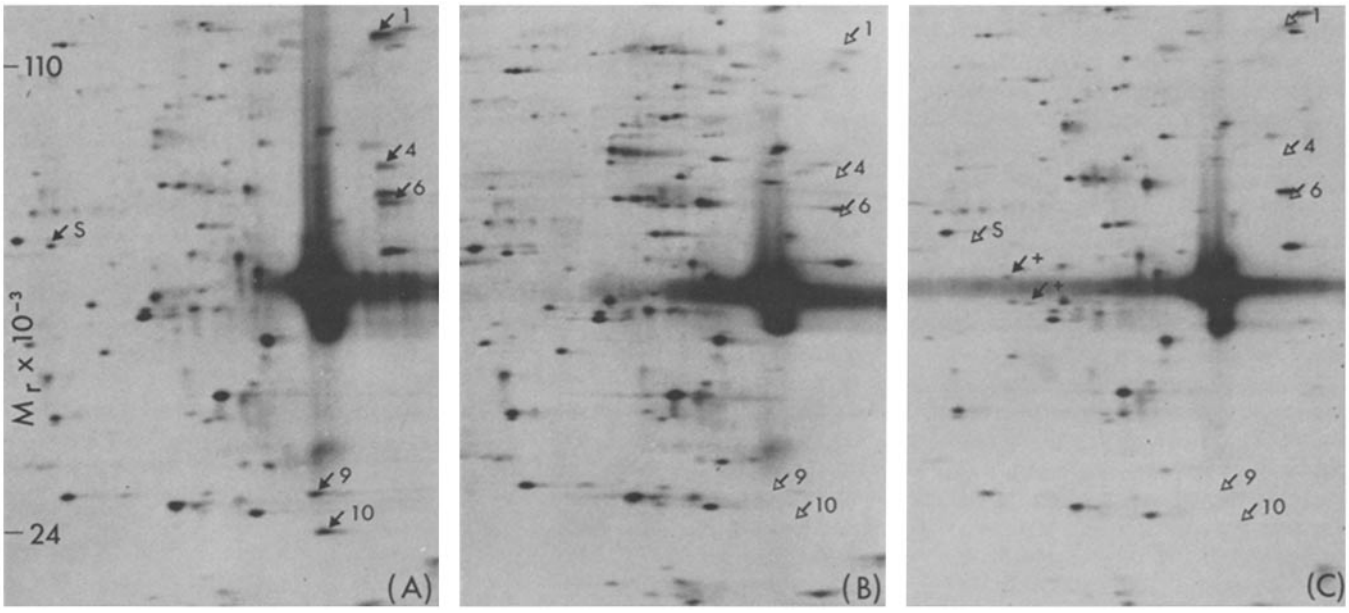

FIGURE 7 Autoradiogram of the polyacrylamide slab gels used for the two-dimensional separation of ^{35}S-labeled axonemal polypeptides. Methods of cell culture, radioactive labeling, axonemal isolation, and two-dimensional separation have been previously described (13, 18, 20). Only the relevant portions of the original maps are shown. Proteins were applied to the anodic (right hand) side and basic polypeptides are located on the left side of the gel sab. Tubulins, the preponderant axonemal polypeptides, are overloaded to permit identification of minor polypeptides; the α and β subunits are not resolved, and together form streaks. (*A*) *uni*-1 axonemes. (*B*) sup_{pf}-1 *pf*-17 *uni*-1·7B axonemes. (*C*) sup_{pf}-3 *pf*-17 *uni*-1·1B axonemes. The numbers and symbols are described in the text.

mutant strains used for analysis of flagellar motility and cultured them under the same conditions used for the motility studies. It has been established that axonemes of the radial-spokehead deficient mutants *pf*-1 and *pf*-17 lacked five polypeptides ranging in molecular weight from 123,000 to 24,000 (14, 19). These polypeptides are a constant feature of wild-type axonemes and have a characteristic position in two-dimensional electrophoretic maps generated by nonequilibrium pH gradient electrophoresis followed by acrylamide gradient gel electrophoresis in SDS. In the same two-dimensional maps, sup_{pf}-3 shows specific alterations, and in one-dimensional electrophoretic gels used to resolve polypeptides of ~300,000 mol wt (20) sup_{pf}-1 has a specific alteration (15). Using these specific molecular phenotypes we could confirm the presence of the sup_{pf} and *pf*-17 mutations in the recombinant strains analyzed for their flagellar motility phenotypes.

The results of axonemal analysis are shown in Figs. 7 and 8. No polypeptide defects have been detected in *uni*-1 so that axonemal two-dimensional maps (Fig. 7*A*) and one-dimensional electrophoreses (Fig. 8, lane *1*) derived from this strain serve as wild-type standards. Comparable analyses of axonemal polypeptides from the recombinant strain sup_{pf}-1 *pf*-17 *uni*-1·7*B* show that radial-spokehead polypeptides 1, 4, 6, 9, and 10 are absent (Fig. 7*B*) and that the altered electrophoretic mobility of high molecular weight polypeptide II (Fig. 8, lane *2*) which characterizes sup_{pf}-1 (15) is present. Analysis of the recombinant strain sup_{pf}-3 *pf*-17 *uni*-1·1B shows (Fig. 7*C*) the absence of radial spokehead components 1, 4, 6, 9, and 10, and in addition the absence of a polypeptide "s" regularly present in wild-type along with the appearance of two new polypeptides (indicated with plus signs in Fig. 7*C*). The latter changes are characteristic of sup_{pf}-3 (15). As expected the sup_{pf}-3 *pf*-17 *uni*-1 recombinant shows no alteration in high molecular weight polypeptides (Fig. 8, lane *3*).

The alterations in the sup_{pf} *pf*-17 *uni*-1 recombinant axonemal polypeptides shown in Figs. 7 and 8 were also apparent in preparation of whole flagella (as opposed to demembranated axonemes) analyzed by the same methods (data not shown). In addition, electron microscopic study of axonemes from the two recombinant strains showed them to have the typical appearance of spokehead deficient mutants (14, 19).

DISCUSSION

Wild-Type Bending Pattern

Our use of a uniflagellar mutation, *uni*-1, has made it easy to obtain high-quality photographs of the flagellar bending pattern of *Chlamydomonas*, so that we have been able to carry out a more detailed analysis of the wild-type bending pattern than has been possible previously. Our photographs and composite tracings of flagella on uniflagellate cells show flagellar configurations indistinguishable from those described in previous studies of flagella on biflagellate cells (16, 22). We therefore have no reason to believe that the uniflagellate condition is associated with any alterations in flagellar motility, and we will consider that the data we have obtained from cells containing *uni*-1 provide information about the wild-type flagellar bending pattern.

As recognized by the earlier studies, the wild-type bending pattern of *Chlamydomonas* is a highly asymmetric bending pattern resembling ciliary bending patterns (25). The beat cycle can be considered to consist of two phases, an effective phase in which a principal bend forms near the basal end of the flagellum while the relatively straight distal region of the flagellum sweeps through the water, and a recovery phase in which the principal bend formed near the base propagates distally, leaving the flagellum nearly straight and pointed anteriorly. Examination of the shear curves, such as Fig. 2*a*, makes it clear that the flagellum also generates reverse bends, which propagate along the flagellum in alternation with the principal bends. It may be important to consider these regions as reverse bends, even though their average curvature is only slightly different from 0, rather than as straight regions, as they have traditionally been regarded in analyses of ciliary movement.

The shear curves make it evident that the principal and reverse bends are also regions in which the sliding between flagellar microtubules occurs in different directions. For convenience, we use P-sliding to refer to sliding in the direction which occurs in principal bends, causing them to propagate distally, and R-sliding to refer to sliding in the direction which occurs in reverse bends. Generation of flagellar bending waves by the continuous propagation of alternating regions of P- and R-sliding has previously been designated as a metachronous sliding pattern (7, 10). In particular, our shear curves show that the initiation of the effective stroke in *Chlamydomonas* flagella corresponds to the initiation of R-sliding that is restricted to the reverse bend region, with P-sliding continuing at approximately the same rate in the principal bend near the tip of the flagellum. Previous analyses of ciliary bending patterns have emphasized the need for a synchronous activation of R-sliding throughout the length of the cilium at the beginning of the effective stroke (21). Our observations suggest that there is no fundamental difference in control mechanisms between cilia and *Chlamydomonas* flagella. In both cases, a synchronous activation of R-sliding appears to be needed throughout the length of the reverse bend; in the case of *Chlamydomonas* flagella, there is usually a principal bend near the tip of the flagellum at the time of initiation of R-sliding, so that it is possible to see that the sliding in this principal bend is not altered.

The shear curves obtained for wild-type flagella of *Chlamydomonas* closely resemble the pattern of shear seen in the basal region (0–15 μm from the base) of sea urchin sperm flagella that have been demembranated and reactivated at a high Ca^{2+} concentration to induce asymmetry (5), with one exception. In the sea urchin sperm flagella, principal bends increase in length and decrease in curvature as they propagate away from the base of the flagellum; we did not find that happening with the *Chlamydomonas* flagella. In the asymmetrically beating sea urchin sperm flagella, synchronous sliding appeared to occur, causing a marked constriction in the amplitude of the shear curves in the region 15–25 μ from the base of the flagellum. The *Chlamydomonas* flagella are too short to show such an effect.

One unusual feature of the wild-type bending pattern of *Chlamydomonas* is the asymmetry in sliding velocities; the sliding velocities in principal bends are ~66% greater than in reverse bends. Since each point on the flagellum must experience equal amounts of P- and R-sliding in each beat cycle, at least on the average, to avoid accumulating shear, the inequality in shear rates must be balanced by an inequality in the length of time a particular point is in a reverse bend or a principal bend. In other words, the reverse bends must be longer than the principal bends; consequently, the asymmetry in bend angle will be less than the asymmetry in average

curvature. This complex of asymmetries is not seen in the asymmetric bending patterns of sea urchin sperm flagella, which appear to maintain principal and reverse bends of equal length (5, 11).

One of the simplest ways to generate an asymmetric bending pattern might be to impose a constant curvature on the flagellum, and then propagate a pattern of symmetric, metachronous sliding on this curved flagellum. In the analysis of asymmetric bending waves in sea urchin sperm flagella by Brokaw (5), this simple possibility appeared to be excluded by the appearance of "synchronous sliding" in the shear curves. Although there is no synchronous sliding apparent in the shear curves obtained with these short flagella on *Chlamydomonas*, the asymmetry in the rates of P- and R-sliding which was found with the *Chlamydomonas* flagella also makes it impossible to generate these bending patterns by a simple superposition of symmetric wave propagation on a curved flagellum.

To extract a characteristic set of parameters from the shear curves, we employed a constant curvature model, which assumes an idealized pattern of metachronous sliding, with P- and R-sliding rates that are constant in time and with position within a bent region. This is only a rough approximation to the actual shear curves, and there are several features of the shear curves that are not represented in this model, and may be significant. Probably the most obvious difference is that the transitions between principal and reverse bends are not abrupt, as in the constant curvature model, but are more gradual. However, we do not find that the transitions involve distinct "straight regions" (of constant shear angle) as suggested in earlier studies of sperm flagellar bending patterns (4, 5). Abrupt transitions are, in fact, unlikely if the flagella have significant elastic bending resistance, as they would require an extremely high active shear moment to be generated in a short region, to change the curvature of the flagellum abruptly.

Another feature of the shear curves that is not represented in the constant curvature model is a higher-than-average curvature in the reverse bend during the initial portion of its development. The curvature then drops rapidly to a low value when R-sliding begins in the reverse bend. This feature is characteristic of the asymmetric bending waves of sea urchin sperm flagella (see Fig. 10 in reference 5). It is a more variable and less pronounced feature of the asymmetric bending patterns of *Chlamydomonas* flagella. In the samples we examined, it appeared to be more pronounced in flagella with lower beat frequencies, (contrast Figs. 3*A* and *B*) including most of the flagella of cells containing sup_{pf}-3 (data not shown).

Finally, many of the shear curves reveal a reduction in the rate of R-sliding as reverse bends approach the distal end of the flagellum, in contrast to the constant sliding velocity assumed by the constant curvature model. The effect of this feature is to restrict the total amount of shear at the distal end of the flagellum to about −3.5 radians.

A similar wild-type bending pattern is also expressed by flagella on cells containing sup_{pf}-1 or sup_{pf}-3, the only difference being that the sup_{pf}-1 flagella have a lower beat frequency, which is approximately half the normal beat frequency. In combination with other evidence (15) this suggests that the outer dynein arms in sup_{pf}-1 flagella may be nonfunctional, and that the inner dynein arms may be sufficient to generate a normal, asymmetric, wild-type bending pattern.

Mutant Bending Pattern

Here we have examined the flagellar bending patterns of two mutant cell types in which the paralyzed flagellar mutant *pf*-17 is combined with one of two suppressor mutations. As described here and in Huang et al. (15), the ultrastructural and biochemical defects associated with the *pf*-17 mutation are retained when combined with these suppressors. Our results show that although these suppressors restore motility in the presence of these *pf*-17 defects, the pattern of motility is distinctly different from wild-type. Differences are easily seen by examining either the bending patterns or the shear curves. These show that the configuration of the flagellum at the end of the effective stroke is somewhat similar in both the mutant and wild-type bending patterns. During the recovery stroke of the mutant flagella, the propagation of the principal bend is associated with the formation of a reverse bend with much greater curvature and bend angle than in the wild-type flagella, and the curvature of the reverse bend is maintained as the reverse bend propagates after R-sliding is initiated.

While photographing *uni*-1 cells and recombinants with *uni*-1 we noted that the single flagellum often tended to attach to the glass surfaces and that cells rotating stably with the flagellum bending in a plane parallel to the microscope-slide surface represented only a fraction of the cell population. In the case of recombinants with *pf*-17 the occurrence of cells attached to the glass by the flagellar tip and of those rotating intermittently was especially frequent, and it was much more difficult to obtain photographs than for other cells containing *uni*-1. We were therefore concerned about whether the small population of cells we were able to photograph was representative of the entire population of mutant cells. Visual observations of large numbers of sup_{pf} *pf*-17 recombinants, both with one and two flagella, convinced us that the bending patterns of these cells were at least superficially similar to those obtained from our photographs, and quite unlike the wild-type pattern. On the other hand, it is likely that our requirements for photography of sup_{pf} *pf*-17 *uni*-1 recombinants select those cells which have the most asymmetric bending patterns, and are therefore most likely to rotate. We conclude that the characteristic mutant bending pattern is probably a nearly symmetric pattern, in which the principal and reverse bends may have nearly equal curvatures. Examples such as the one in Fig. 5*C*, which has a nearly symmetric bending pattern, may be most nearly characteristic of the mutant bending pattern. Examples in which the bending pattern of the mutant flagella is much closer to the wild-type pattern (Fig. 5*B*) cannot safely be cited as evidence for the capability for these flagella to generate the wild-type bending pattern in the presence of the ultrastructural and biochemical deficiencies associated with the *pf*-17 mutation. These few cases with nearly wild-type flagella could represent unique individuals in which the *pf*-17 ultrastructural and biochemical deficiencies may be at least partially restored by some leakiness of the mutation; because of the rarity of this class, the restoration would not be detected in our ultrastructural and biochemical examination of the recombinant population.

If, as suggested above, our photographs of the mutant flagella select a range of phenotypes intermediate between the wild-type and mutant bending patterns, they provide information that would not be obtained from an unbiased sample of the mutant flagella. Data for the sample of sup_{pf}-3 *pf*-17 cells (Table II) show that the average value of κ_R is intermediate between the wild-type value and the value for the sup_{pf}-1 *pf*-17 cells; in addition, the ratio between V_P and V_R (1.22) is also intermediate between the values of 1.7 and 0.98 found for the wild-type and sup_{pf}-1 *pf*-17 samples, respectively. In other words, a

gradual increase in the value of κ_R is associated with a gradual increase in the relative value of V_R, suggesting that there is a coordinated change in both of these variables as the influence of the radial spoke system is gradually decreased.

If the mutant bending pattern of *pf*-17 in the presence of these suppressors is a symmetrical bending pattern, it is important to note that it is very different from the symmetrical bending pattern shown in Fig. 1 *F*, which is obtained during the reversal response of *Chlamydomonas* flagella. The mutant bending pattern clearly involves much larger bend angles. It will be interesting to compare these two symmetrical patterns in detail, and to examine whether the suppressed *pf*-17 cells can display reversal responses, and if so whether the bending

The Function of the Radial-spoke System

The *pf*-17 mutation is characterized by an ultrastructural deficiency in the spokeheads by which the radial spokes interact with central-pair microtubule structures (14), and this deficiency is retained in the presence of the suppressors sup_{pf}-1 and sup_{pf}-3 which restore motility. We therefore conclude that the mutant bending pattern illustrates motility that can be generated by flagella in the absence of a functional radial-spoke system. We can therefore exclude some possible functions that have been suggested for the radial spoke system.

It has been suggested that radial spoke–central tubule interactions are required for conversion of active sliding, generated by the dynein arms between outer doublet microtubules, into bending of the axoneme (27). Our results demonstrate unequivocally that this is incorrect. Bending of the axoneme is necessarily associated with differences in the rates of sliding at different points along the axoneme. These differences in sliding rates can be generated by differences in dynein-arm activity, by the differences in viscous and elastic resistive forces associated with a bending wave, and by sliding resistances imposed by axonemal structures. Since removal of the basal end of an axoneme often prevents conversion of sliding into bending (6, 26), the resistance provided by interconnections of the flagellar microtubules at the basal end of the flagellum appears to be important. Sliding resistances contributed by the radial-spoke system could contribute to or modify the formation of bends, but do not appear to be essential for the conversion of sliding into bending.

Our results also show that, in the absence of a functional radial-spoke system, bends can propagate normally along a flagellum, new bends can develop at the basal end of a flagellum, and an approximately normal flagellar configuration seen at the end of the effective stroke, when P-sliding is initiated, can be reached. The mutant bending pattern seen in the absence of a functional radial-spoke system is a nearly symmetric pattern, similar in many respects to the pattern of bending seen near the basal ends of longer flagella generating waves of large bend angle (12). It may be reasonable to consider it to be a simpler bending pattern than the wild-type bending pattern. The function of the radial-spoke system would then appear to be to modify this simple symmetric bending pattern to produce the asymmetric bending pattern required for effective motility of *Chlamydomonas*.

In the wild-type bending pattern, the flagellum starts its effective stroke from an approximately straight configuration, with little curvature in the reverse bend, and the amount of sliding required to reach the configuration at the end of the effective phase is less than in the mutant bending pattern. Consequently, if the rate of R-sliding is the same, the duration of the effective phase will be less in the wild-type pattern, and the beat frequency can be higher. However, the amount of sliding required to propagate the principal bend to the end of the flagellum will be the same, regardless of the curvature in the reverse bend. Consequently, the duration of the recovery phase will remain the same if the rate of P-sliding is the same, and the recovery phase will occupy about two-thirds of the beat cycle. This is not what is seen in the wild-type pattern. Instead, the rate of P-sliding is higher, so that the duration of the recovery phase is similar to the duration of the effective phase, and the beat frequency is further increased over that found with the mutant bending pattern.

This pattern of changes in bending pattern which we are attributing to the functioning of the radial spoke system differs from that seen when asymmetry is induced in sea urchin sperm flagella by an increase in Ca^{2+} concentration (5). In the latter case, the curvature in the reverse bends can be reduced to 0, but this is not associated with an increase in the rate of P-sliding. Instead, there is an increase in curvature in the principal bends, and no change in beat frequency.

Although it is relatively easy to imagine that the radial-spoke system could monitor the curvature of the flagellum, and interact with the central pair microtubule system in a way that would limit the curvature that develops in the reverse bends, it is less easy to understand the increased rate of P-sliding that is observed in the presence of the functional radial-spoke system. This second effect could independently be a direct effect of the radial spoke system. More likely, it may indicate the presence of a separate regulatory mechanism in the flagellum, perhaps one that adjusts the relative lengths of the recovery and effective phases by increasing the rate of P-sliding. Further understanding of these changes in bending pattern will probably require detailed simulation of models for the bending of *Chlamydomonas* flagella that take into account the various resistances that may influence the rate of P-sliding and examine various types of control mechanisms.

The primary action of the radial-spoke system in converting a symmetric bending pattern into the asymmetric, wild-type bending pattern appears to be an inhibition of the development of reverse bends. In the paralyzed mutants with radial-spoke system defects, both principal and reverse bend initiation appear to be inhibited. However, these two types of inhibition must be different, since sup_{pf} mutations overcome the inhibition of bending associated with radial-spoke system defects, but do not block the inhibition of reverse bending in the wild-type bending pattern.

We thank Zenta Remanis for making the recombinant strains and for characterizing them genetically, Sandy Nakada for assistance with photographic processing and data analysis, and Drs. I. R. Gibbons and C. Omoto for comments on an early version of this manuscript.

This work has been supported by National Institutes of Health research grants GM-17132, GM-18711 and GM-25965.

Received for publication 31 August 1981, and in revised form 9 November 1981.

REFERENCES

1. Allen, C., and G. G. Borisy. 1974. Flagellar motility in *Chlamydomonas*: reactivation and sliding in vitro. *J. Cell Biol.* 63:5*a* (Abstr.).
2. Asai, D. J., and C. J. Brokaw. 1980. Effects of antibodies against tubulin on the movement of reactivated sea urchin sperm flagella. *J. Cell Biol.* 87:114–123.
3. Brokaw, C. J. 1963. Movement of the flagella of *Polytoma uvella*. *J. Exp. Biol.* 40: 149–156.
4. Brokaw, C. J. 1965. Non-sinusoidal bending waves of sperm flagella. *J. Exp. Biol.* 43:155–169.

5. Brokaw, C. J. 1979. Calcium-induced asymmetrical beating of Triton-demembranated sea urchin sperm flagella. *J. Cell Biol.* 82:401–411.
6. Brokaw, C. J., and B. Benedict. 1968. Mechanochemical coupling in flagella. I. Movement-dependent dephosphorylation of ATP by glycerinated spermatozoa. *Arch. Biochem. Biophys.* 125:770–778.
7. Brokaw, C. J., and I. R. Gibbons. 1975. Mechanisms of movement in flagella and cilia. *In* Swimming and Flying in Nature. T. Y.-T. Wu, C. J. Brokaw, and C. Brennan, editors. Plenum Publishing Corp., New York. 89–126.
8. Brokaw, C. J., and T. F. Simonick. 1976. CO_2 regulation of the amplitude of flagellar bending. *In* Cell Motility. R. D. Goldman, T. D. Pollard, and J. L. Rosenbaum, editors. Cold Spring Harbor Laboratory, Cold Spring Harbor, N. Y. 933–940.
9. Gibbons, B. H., and I. R. Gibbons. 1972. Flagellar movement and adenosine triphosphatase activity in sea urchin sperm extracted with Triton X-100. *J. Cell Biol.* 54:75–97.
10. Goldstein, S. F. 1976. Form of developing bends in reactivated sperm flagella. *J. Exp. Biol.* 64:173–184.
11. Goldstein, S. F. 1977. Asymmetric waveforms in echinoderm sperm flagella. *J. Exp. Biol.* 71:157–170.
12. Hiramoto, Y., and S. A. Baba. 1978. A quantitative analysis of flagellar movement in echinoderm spermatozoa. *J. Exp. Biol.* 76:85–104.
13. Huang, B., G. Piperno, and D. J. L. Luck. 1979. Paralyzed flagella mutants of *Chlamydomonas reinhardtii*: defective for axonemal doublet microtubule arms. *J. Biol. Chem.* 254:3091–3099.
14. Huang, B., G. Piperno, Z. Ramanis, and D. J. L. Luck. 1981. Radial spokes of *Chlamydomonas* flagella: genetic analysis of assembly and function. *J. Cell. Biol.* 88:80–88.
15. Huang, B., Z. Ramanis, and D. J. L. Luck. 1982. Suppressor mutations in *Chlamydomonas* reveal a regulatory mechanism for flagellar function. *Cell.* 28:115–124.
16. Hyams, J. S., and G. G. Borisy. 1978. Isolated flagellar apparatus of *Chlamydomonas*: characterization of forward swimming and alteration of waveform and reversal of motion by calcium ions in vitro. *J. Cell Sci.* 33:235–253.
17. Lindemann, C. B., I. Fentie, and R. Rikmenspoel. 1980. A selective effect of Ni^{2+} on wave initiation in bull sperm flagella. *J. Cell Biol.* 87:420–426.
18. Luck, D. J. L., G. Piperno, Z. Ramanis, and B. Huang. 1977. Flagellar mutants of *Chlamydomonas*: studies of radial spoke–defective strains by dikaryon and revertant analysis. *Proc. Natl. Acad. Sci. U. S. A.* 74:3456–3460.
19. Piperno, G., B. Huang, and D. J. L. Luck. 1977. Two-dimensional analysis of flagellar proteins from wild-type and paralyzed mutants of *Chlamydomonas reinhardtii*. *Proc. Natl. Acad. Sci. U. S. A.* 74:1600–1604.
20. Piperno, G., and D. J. L. Luck. 1979. Axonemal adenosine triphosphatases from flagella of *Chlamydomonas reinhardtii*. Purification of two dyneins. *J. Biol. Chem.* 254:3084–3090.
21. Rikmenspoel, R., and M. A. Sleigh. 1970. Bending moments and elastic constants in cilia. *J. Theor. Biol.* 28:81–100.
22. Ringo, D. L. 1967. Flagellar motion and fine structure of the flagellar apparatus in *Chlamydomonas*. *J. Cell Biol.* 33:543–571.
23. Schmidt, J. A., and R. Eckert. 1976. Calcium couples flagellar reversal to photostimulation in *Chlamydomonas reinhardtii*. *Nature (Lond.).* 262:713–715.
24. Shingyoji, C., A. Murakami, and K. Takahashi. 1977. Local reactivation of Triton-extracted flagella by iontophoretic application of ATP. *Nature (Lond.).* 265:269–270.
25. Sleigh, M. A. 1968. Patterns of ciliary beating. *Symp. Soc. Exp. Biol.* 32:131–150.
26. Summers, K. E., and I. R. Gibbons. 1971. Adenosine-triphosphate-induced sliding of tubules in trypsin-treated flagella of sea urchin sperm. *Proc. Natl. Acad. Sci. U. S. A.* 68: 3092–3096.
27. Warner, F. D., and P. Satir. 1974. The structural basis of ciliary bend formation. *J. Cell Biol.* 63:35–63.
28. Warr, J. R., A. McVittae, J. Randall, and J. M. Hopkins. 1966. Genetic control of flagellar structure in *Chlamydomonas reinhardtii*. *Genet. Res.* 7:335–351.
29. Witman, G. B., R. Fay, and J. Plummer. 1976. *Chlamydomonas* mutants: evidence for the roles of specific axonemal components in flagellar movement. *In* Cell Motility. R. D. Goldman, T. D. Pollard, and J. L. Rosenbaum, editors. Cold Spring Harbor Laboratory, Cold Spring Harbor, N. Y. 969–986.
30. Witman, G. B., J. Plummer, and G. Sander. 1978. *Chlamydomonas* flagellar mutants lacking radial spokes and central tubules. *J. Cell Biol.* 76:729–747.